Nucleic Acids Research, 2005, Vol. 33, No. 7 ***2061–2077***
doi:10.1093/nar/gki336

NMR chemical shift and relaxation measurements provide evidence for the coupled folding and binding of the p53 transactivation domain

Pamela D. Vise, Bharat Baral, Andrew J. Latos and Gary W. Daughdrill*

Department of Microbiology, Molecular Biology and Biochemistry, University of Idaho, PO Box 443052, Life Science South Room 142, Moscow 83844-3052, Idaho

Received January 7, 2005; Revised and Accepted March 16, 2005

ABSTRACT

The interaction between the acidic transactivation domain of the human tumor suppressor protein p53 (p53TAD) and the 70 kDa subunit of human replication protein A (hRPA70) was investigated using heteronuclear magnetic resonance spectroscopy. A $^{1}H–^{15}N$ heteronuclear single quantum coherence (HSQC) titration experiment was performed on a ^{15}N-labeled fragment of hRPA70, containing the N-terminal 168 residues ($hRPA70_{1–168}$) and p53TAD. $HRPA70_{1–168}$ residues important for binding were identified and found to be localized to a prominent basic cleft. This binding site overlapped with a previously identified single-stranded DNA-binding site, suggesting that a competitive binding mechanism may regulate the formation of p53TAD–hRPA70 complex. The amide ^{1}H and ^{15}N chemical shifts of an uniformly ^{15}N-labeled sample of p53TAD were also monitored before and after the addition of unlabeled $hRPA70_{1–168}$. In the presence of unlabeled $hRPA70_{1–168}$, resonance lineshapes increased and corresponding intensity reductions were observed for specific p53TAD residues. The largest intensity reductions were observed for p53TAD residues 42–56. Minimal binding was observed between p53TAD and a mutant form of $hRPA70_{1–168}$, where the basic cleft residue R41 was changed to a glutamic acid (R41E), demonstrating that ionic interactions play an important role in specifying the binding interface. The region of p53TAD most affected by binding $hRPA70_{1–168}$ was found to have some residual alpha helical and beta strand structure; however, this structure was not stabilized by binding $hRPA70_{1–168}$. ^{15}N relaxation experiments were performed to monitor changes in backbone dynamics of p53TAD when bound to $hRPA70_{1–168}$. Large changes in both the transverse (R_2) and rotating frame ($R_{1\rho}$) relaxation rates were observed for a subset of the p53TAD residues that had $^{1}H–^{15}N$ HSQC resonance intensity reductions during the complex formation. The folding of p53TAD upon complex formation is suggested by the pattern of changes observed for both R_2 and $R_{1\rho}$. A model that couples the formation of a weak encounter complex between p53TAD and $hRPA70_{1–168}$ to the folding of p53TAD is discussed in the context of a functional role for the p53–hRPA70 complex in DNA repair.

INTRODUCTION

To promote the preservation and damage-free replication of genomic DNA, a complex system of proteins that can efficiently recognize and repair the most frequently occurring types of DNA damage has evolved (1–4). The four principle DNA repair systems for eukaryotic genomes are base excision repair, mismatch repair, nucleotide excision repair and recombinational repair. In humans, the four DNA repair systems share many features, including overlapping substrate specificity and proteins that are used in multiple repair pathways (3,5). Human replication protein A (hRPA) is a heterotrimeric single-stranded (ssDNA)-binding protein that is required for base excision repair, nucleotide excision repair and recombinational repair (3,5,6). HRPA is composed of 32 kDa (hRPA32), 14 kDa (hRPA14) and 70 kDa (hRPA70) subunits (7,8). A linear schematic representation of the hRPA70 subunit is shown at the top of Figure 1. The first 180 residues of hRPA70 consists of a structured domain that forms an oligonucleotide binding fold known as DNA-binding domain F (DBD F) (residues 1–105) and a flexible linker (residues 106–180) (9). DBD F contains a weak ssDNA-binding site that is localized to a prominent basic cleft (9,10). The positively charged residues comprising the basic cleft are underlined in the hRPA70 primary sequence for residues 1–168 (Figure 1). DBD F is also the site for many of the interactions

*To whom correspondence should be addressed. Tel: +1 208 885 9230; Fax: +1 208 885 6518; Email: gdaugh@uidaho.edu

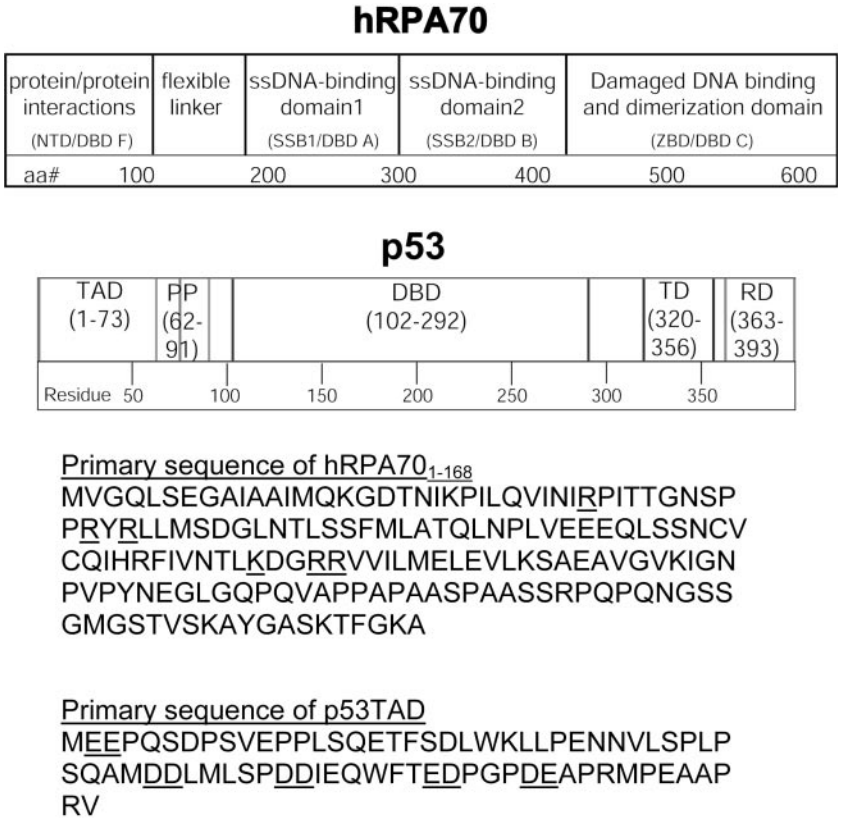

Figure 1. Linear schematic diagrams showing the functional domains of hRPA70 and p53. Beneath the schematic diagrams are the primary sequences of $hRPA70_{1-168}$ and p53TAD. The $hRPA70_{1-168}$ basic cleft residues and the p53TAD negatively charged residue pairs are underlined in each sequence.

that occur between hRPA70 and other proteins during DNA metabolism (9,11–14). The flexible linker connects DBD F to two tandem, high-affinity ssDNA-binding domains (DBD A and B, residues 181–422) that also have oligonucleotide binding topologies (15). C-terminal of DBD B is a domain that is important for dimerization with hRPA32 and this domain may also participate in the recognition of the bulky DNA adducts that are repaired during nucleotide excision repair (DBD C, residues 423–614) (5,15–19).

HRPA has numerous protein-binding partners that are important for its functions during DNA repair (5,13,20). One protein that binds hRPA is the human tumor suppressor protein, p53 (13,21–24). The hRPA–p53 complex disassociates in response to DNA damage and in the presence of ssDNA (21,24). It is hypothesized that the hRPA–p53 complex provides a reservoir of p53 that is immediately available during the early stages of DNA repair (24). The p53 protein regulates the cell cycle in response to a variety of stress signals, primarily through direct transcriptional activation or repression of specific target genes (25–27). The specific stress signal as well as the cell type and context will dictate whether p53 induces transient growth arrest, or senescence or apoptosis. In response to UV radiation, p53 induces a transient growth arrest that provides the DNA repair machinery the necessary time to repair the damage. After repair is completed, there is a c-Jun-mediated exit back to the cell cycle (28). It also appears that p53 can play a more direct role in DNA repair and replication (29,30). Figure 1 shows a linear schematic representation of p53 containing five functional domains, the transactivation domain (TAD) (residues 1–73), the polyproline region (PP) (residues 62–91), the sequence-specific DBD (residues 102–292), the tetramerization domain (TD) (residues 320–356) and the regulatory domain (RD) (residues 363–393). The TAD contains several sites for phosporylation, some of which prevent p53 from targeted degradation (31). The PP domain contains five partially conserved PXXP repeats and is necessary for efficient growth suppression (32). The DBD is responsible for site-specific DNA binding and is the domain where many cancer associated mutations are found (33,34). The TD is essential for p53 tetramerization, which appears to be necessary for the phosphorylation of certain sites in the TAD but not for site-specific DNA binding (35). The RD is thought to regulate the function of the DBD (27). The p53 DBD and TD have been well characterized at a molecular level by NMR and X-ray crystallography (36–40). Conversely, the TAD and RD are not well characterized at a structural level. Approximately 50% of full-length p53 is unfolded under native conditions (41,42). The TAD is one such unstructured region (43,44). The ability of intrinsically unstructured proteins (IUPs) to participate in the complex regulatory processes is becoming a new paradigm in molecular biology (41). It is hypothesized that IUPs are pliable and able to remodel their structures to interact with multiple protein partners (45,46).

Affinity chromatography and mutational studies have shown that hRPA70 and not hRPA32 or hRPA14 interacts with p53 (13,22,23). Further, deletion analysis has shown that hRPA70 residues 1–221 are important for this interaction (16). In addition, this study also showed that hRPA70 residues

411–492 can interact with full-length p53, but with a lower affinity than residues 1–221. A series of mutational studies identified regions near the N- and C-termini of p53 that are involved in binding hRPA70 (21–23,47). Truncated versions of p53 consisting of residues 2–71 and 289–356 are able to form a complex with hRPA70 (47). However, four truncated versions of p53 consisting of residues 2–45, 46–71, 289–330 and 331–356 do not bind hRPA70 (47). These studies also showed that p53 residues 40–60 were essential for the formation of the p53–hRPA70 complex (21,47). While the deletion studies reviewed in this section identified specific regions of either p53 or hRPA70 that are necessary for complex formation with the full-length counterpart, they did not identify the minimal domains of both proteins that are sufficient for complex formation. In this study, we present evidence for a direct interaction between the transactivation domain of p53 (residues 1–73, p53TAD) and a fragment of hRPA70 containing DBD F and most of the flexible linker (residues 1–168, $hRPA70_{1–168}$). Site-directed mutations localized to the DBD F and the flexible linker were investigated revealing an hRPA70 motif that is essential for complex formation. Further, $hRPA70_{1–168}$ and p53TAD chemical shift maps are presented, identifying the binding interface for this interaction. This report also includes a detailed examination of the secondary structure and dynamics of p53TAD in the presence and absence of $hRPA70_{1–168}$. In particular, changes in backbone dynamics that occur for specific p53TAD residues upon binding $hRPA70_{1–168}$ suggest a mechanism where the folding of p53TAD is coupled to binding $hRPA70_{1–168}$.

MATERIALS AND METHODS

Media

All growth experiments were performed in M9 media. For the production of isotopically labeled samples 1 g/l of ^{15}N-labeled ammonium chloride and/or 0.2% (w/v) ^{13}C-labeled glucose were added in the place of nitrogen and carbon sources (Cambridge Isotopes). All cells were grown at 37°C.

Expression and purification of p53TAD

A plasmid containing the complete human p53 cDNA was obtained from Dr Lee Fortunato (University of Idaho). The genetic sequence for residues 1–73 of human p53 was amplified by the PCR using two primers d(CGACAAGCATATGATGGAGGAGCCGCAGTCA) and d(AAATCCTCGAGTCACACGCGGGGAGCAGC). The product of this reaction was digested with NdeI at the 5′ end and XhoI at the 3′ end and subcloned into pET28a (Novagen). This yielded a vector where residues 1–73 of human p53 could be expressed with an N-terminal 7-histidine tag and a thrombin cleavage site. The identity of this clone was verified by DNA sequencing.

The p53/pET28a clone was transformed into Ca^{2+}-treated *Escherichia coli* BL21(DE3) cells using the heat-shock method (Novagen). Single colonies from this transformation were used to inoculate 50 ml cultures of M9 media that were grown overnight. The overnight cultures were then re-inoculated into 2 L of M9 media at an A_{600} of 0.03. These cultures were induced at an A_{600} of 0.7 with 1 mM isopropyl-β-D-thiogalactopyranoside and grown for 6 h. The pelleted cells were resuspended in 35 ml of lysis buffer (50 mM NaH_2PO_4, 300 mM NaCl, 10 mM imidazole and 0.02% NaN_3, pH 8.0) containing protease inhibitors (Sigma) and lysed using a French press. The clarified lysate was loaded onto a column containing 30 ml of NiNATA Superflow resin (Qiagen) that had previously been equilibrated with 5 column volumes of lysis buffer. All buffers used on the NiNATA column were run at a flow rate of 3 ml/min. The column was washed with 2 column volumes of wash buffer (50 mM NaH_2PO_4, 300 mM NaCl, 20 mM imidazole and 0.02% NaN_3, pH 8.0) and the p53 eluted with 3 column volumes of elution buffer (50 mM NaH_2PO_4, 300 mM NaCl, 250 mM imidazole, 0.02 % NaN_3, pH 8.0). Fractions were analyzed using PAGE and those containing the protein were combined and dialyzed into the gel filtration buffer (50 mM NaH_2PO_4, 300 mM NaCl, 1 mM EDTA and 0.02% NaN_3, pH 7.0) using 3500 Da MWCO dialysis tubing (Spectrapor). The p53 protein was then concentrated in a centriprep YM3 (Amicon) and the histidine tag cleaved by thrombin (thrombin clean cleave kit, RECOM-T; Sigma). To achieve optimal cleavage, the protein was incubated with thrombin for 2 h at room temperature. The completion of the cleavage reaction was verified using PAGE. The p53 protein was then loaded onto a HiLoad 16/60 Superdex 75 prep grade column (Pharmacia). The column was equilibrated and the protein eluted with gel-filtration buffer at a flow rate of 1.5 ml/min. Protein purity was verified using PAGE analysis. The purified p53 protein was dialyzed into the NMR experiment buffer; 50 mM NaH_2PO_4, 50 mM NaCl, 1 mM EDTA and 0.02% NaN_3 and 1 mM DTT, pH 6.5 and concentrated in a YM3 centriprep/centricon (Amicon).

Expression and purification of $hRPA70_{1–168}$

Expression and purification of $hRPA70_{1–168}$ was based on a published protocol (48). A clone containing the cDNA corresponding to amino acid residues 1–168 of hRPA70 in pet11d ($hRPA70_{1–168}$) was described previously (12). *E.coli* BL21DE3 cells containing the $hRPA70_{1–168}$ plasmid were used to inoculate a 50 ml overnight culture. This culture was diluted into 2 L M9 media at A_{600} of 0.03. The 2 L culture was induced with 1 mM isopropyl-β-D-thiogalactopyranoside at an A_{600} of 0.6 and grown for 3 h. Pelleted cells were resuspended in HI buffer [30 mM HEPES from a 1 M HEPES stock, pH 7.8, 0.25 mM EDTA, 0.25% (w/v) inositol, 0.01% (v/v) IGEPAL and 1 mM DTT] containing 50 mM KCl and protease inhibitors (Sigma). The resuspended cells were lysed using a French press and the supernatant was isolated by centrifugation. The supernatant was loaded onto a column containing 30 ml of Affi-gel blue resin (Biorad) equilibrated with 5 column volumes of HI buffer containing 50 mM KCl. All buffers used on this column were at a flow rate of 3 ml/min. The column was washed sequentially with 4 column volumes of HI buffer plus 0.8 M KCl, 4 column volumes of HI buffer plus 0.5 M NaSCN, 3 column volumes of HI buffer plus 1.0 M NaSCN and 3 column volumes of HI buffer plus 1.5 M NaSCN. The protein is eluted in the 1.5 M NaSCN step. The fractions were analyzed using PAGE and fractions containing $hRPA70_{1–168}$ were pooled and dialyzed into the gel filtration buffer (50 mM NaH_2PO_4, 1 mM EDTA, 300 mM NaCl and 0.02% NaN_3, pH 7.0). The protein was further purified on a size exclusion column (HiLoad 16/60 Superdex

75 prep grade column; Pharmacia) using the gel-filtration buffer. Following gel filtration, $hRPA70_{1–168}$ purity was determined using PAGE. Fractions containing $hRPA70_{1–168}$ were dialyzed into the NMR experiment buffer and concentrated using a YM10 centriprep/centricon (Amicon).

Two mutants containing single amino acid changes were made in the $hRPA70_{1–168}$ clone described above. The clones contained either an Y118A or a R41E mutation and are referred to as Y118A and R41E. The mutations were made by following the procedure outlined in the Stratagene Site Directed Mutagenesis Kit and the identity of each clone was verified by DNA sequencing. Y118A and R41E were overexpressed and purified using the same method as described for $hRPA70_{1–168}$.

NMR data collection and analysis

All NMR experiments were performed on a Varian Inova spectrometer operating at a ^{1}H resonance frequency of 600 MHz and a sample temperature of either 278 or 298K. To make the amide ^{1}H and ^{15}N as well as $^{13}C^{\alpha}$, $^{13}C^{\beta}$ and ^{13}CO resonance assignments, sensitivity enhanced HNCACB and HNCO experiments were performed on a 0.30 mM uniformly ^{15}N and ^{13}C labeled sample of p53TAD in 90% H_2O/10% D_2O using the NMR experiment buffer (49–51). For the HNCACB experiment, data in the ^{1}H dimension was acquired using a sweep width of 8000 Hz and 512 complex t3 points, data in the ^{13}C dimension were acquired using a sweep width of 12 065.5 Hz and 128 complex t1 points, and data in the ^{15}N dimension were acquired using a sweep width of 1400 Hz and 32 complex t2 points. For the HNCO, experimental parameters were identical to the ^{1}H and ^{15}N dimensions of the HNCACB. Data in the ^{13}C dimension of the HNCO were acquired using a sweep width 3017.1 Hz and 64 complex t1 points. Processing and analysis of the HNCACB data resulted in 60 non-proline, amide ^{1}H, ^{15}N, $^{13}C^{\alpha}$ and $^{13}C^{\beta}$ resonance assignments plus 12 proline $^{13}C^{\alpha}$ and $^{13}C^{\beta}$ resonance assignments. Processing and analysis of the HNCO data resulted in 59 ^{13}CO resonance assignments. The $^{1}H^{\alpha}$ resonance assignments were made using the 3D ^{15}N-edited TOCSY-heteronuclear single quantum coherence (HSQC) experiment and a 0.30 mM uniformly ^{15}N-labeled sample of p53TAD (52). For the TOCSY-HSQC experiment, data in the direct ^{1}H dimension were acquired using a sweep width of 8000 Hz and 512 complex t3 points, data in the indirect ^{1}H dimension were acquired with a sweep width of 8000 Hz and 128 complex t1 points and data in the ^{15}N dimension were acquired with a sweep width of 1400 Hz and 32 complex t2 points. Processing and analysis of the TOCSY-HSQC data resulted in 59 non-proline $^{1}H^{\alpha}$ resonance assignments. The $hRPA70_{1–168}$ resonance assignments were described previously (9).

For the p53TAD and $hRPA70_{1–168}$ titration experiments, 2D, gradient enhanced, $^{1}H–^{15}N$ HSQC spectra were acquired on uniformly ^{15}N-labeled samples of p53TAD and $hRPA70_{1–168}$ in NMR experiment buffer (49,53). For the p53TAD $^{1}H–^{15}N$ HSQC experiments, data in the ^{1}H dimension were acquired using a sweep width of 8000 Hz and 512 complex t2 points and data in the ^{15}N dimension were acquired using a sweep width of 1140 Hz and 128 complex t1 points. For the $hRPA70_{1–168}$ $^{1}H–^{15}N$ HSQC experiments, data in the ^{1}H dimension were acquired using a sweep width of 8000 Hz and 512 complex t2 points and data in the ^{15}N dimension were acquired using a sweep width of 2200 Hz and 128 complex t1 points. Titrations were performed using a 0.30 mM uniformly ^{15}N-labeled sample of p53TAD in 90% H_2O/10% D_2O in the NMR experiment buffer. Unlabeled $hRPA70_{1–168}$ at a stock concentration of 0.45 mM was added to the p53TAD sample to concentrations of 0.005, 0.010, 0.050, 0.10, 0.15 and 0.30 mM. After each addition of unlabeled $hRAP70_{1–168}$, a $^{1}H–^{15}N$ HSQC spectrum was collected using the same parameters described above. When enough unlabeled $hRAP70_{1–168}$ was added to increase the total sample volume by 10%, the sample was removed from the NMR tube and concentrated to the original volume (600 µl) using a YM3 centricon. The reverse titration was performed using a 0.60 mM uniformly ^{15}N-labeled sample of $hRPA70_{1–168}$ in 90% H_2O/10% D_2O in the NMR experiment buffer. Unlabeled p53TAD at a stock concentration of 0.45 mM was added to the p53TAD sample to concentrations of 0.005, 0.010, 0.050, 0.10, 0.15, 0.30 and 0.60 mM. Other experimental conditions were identical to those used for the ^{15}N-labeled p53TAD titration. Similar results were observed for titrations both at 278 and at 298K.

All NMR spectra were processed and analyzed using the Felix software from the Accelerys Corporation (Cambridge, MA). Apodization was achieved in the ^{1}H, ^{13}C and ^{15}N dimensions using a squared sine bell function shifted by 90°. Apodization was followed by zero filling to twice the number of real data points and mirror image linear prediction was used in the ^{15}N dimension of the HNCACB. Amide ^{1}H, ^{15}N and ^{13}C chemical shift and resonance peak height measurements were made using the Felix program and converted into tab-delimited ASCII files. Intensity ratio plots were generated using the KaleidaGraph software from Synergy (Reading, PA). The referencing method used in this report is based on IUPAC recommendations for using DSS in a highly polar solvent, such as water (54,55).

Relaxation data collection

The relaxation experiments for free p53TAD were acquired at 298K on 0.30 mM uniformly ^{15}N-labeled sample at pH 6.5 in NMR experiment buffer. In addition, the relaxation experiments for bound p53TAD were acquired under the same conditions after the addition of unlabeled $hRPA70_{1–168}$ to a concentration 0.075 mM. The spin-lattice relaxation rates (R_1), spin–spin relaxation rates (R_2), rotating frame relaxation rates ($R_{1\rho}$) and $^{1}H–^{15}N$ NOEs were measured by inverse-detected 2D NMR methods (56). The spin-lattice relaxation rates were determined by collecting 10 2D spectra using relaxation delays of 10, 50, 110, 190, 310, 500, 650, 1000, 1500 and 1900 ms. The spin–spin relaxation rates and rotating-frame relaxation rates were each determined by collecting 10 2D spectra using relaxation delays of 10, 30, 50, 90, 110, 150, 190, 210, 230 and 250 ms. A 70°, off-resonance, spinlock pulse with a field strength of 1.5 kHz was used for the $R_{1\rho}$ experiments. Peak heights from each series of relaxation experiments were fitted to a single decaying exponential function. To measure the $^{1}H–^{15}N$ NOEs one spectrum was acquired with a 3 s mixing time for the NOE to build up and the another spectrum was acquired with a 3 s recycle delay for a reference. For all experiments water suppression was achieved by using pulsed field gradients. The R_1, R_2, $R_{1\rho}$ and $^{1}H–^{15}N$ NOE values

were determined for all 60 non-proline resonances of free p53TAD and 58 non-proline resonances for p53TAD bound to $hRAP70_{1–168}$. Relaxation data were not determined for E51 and Q52 in p53TAD bound to $hRAP70_{1–168}$ owing to weak resonance intensities. In addition, resonances for W53 and F54 overlap in both free and bound p53TAD at 298K and the relaxation data presented for these residues are an average value. A similar condition exists for Q16 and R72. Uncertainties in measured peak heights were estimated from baseline noise level and were typically <1% of the peak heights from the first R_1, R_2 and $R_{1\rho}$ delay points. In general, fitting errors were within 10% of the calculated relaxation rates.

Relaxation data analysis

Relaxation data were analyzed using the reduced spectral density mapping approach (57–60). The ^{15}N chemical shift anisotropy and the dipolar coupling between the amide ^{15}N nucleus and the attached proton have the greatest influence on the ^{15}N nuclear relaxation (61). The values for R_1, R_2 and the NOE between the amide proton and the nitrogen are related to the spectral density using the following relationships:

$$R_1 = \left(\frac{d^2}{4}\right)[3J(\omega_N) + 6J(\omega_H + \omega_N) + J(\omega_H - \omega_N)] + c^2 J(\omega_N), \quad 1$$

$$R_2 = \left(\frac{d^2}{8}\right)[4J(0) + 3J(\omega_N) + 3J(\omega_H + \omega_N) + 6J(\omega_H) + J(\omega_H - \omega_N)] + \left(\frac{c^2}{6}\right)[J(0) + 6J(\omega_N)] + R_{ex}, \quad 2$$

$$NOE = 1 + \left(\frac{d^2}{4R_1}\right)\left(\frac{\gamma_H}{\gamma_N}\right)[6J(\omega_H + \omega_N) - J(\omega_H - \omega_N)], \quad 3$$

where $d = (\mu_0 h \gamma_H \gamma_N / 8\pi^2)\langle r_{NH}^{-3}\rangle$ and $c = \omega_N \Delta\sigma/\sqrt{3}$, μ_0 is the permeability of free space, h is the Planck's constant, γ_H and γ_N are the gyromagnetic ratios of ^1H and ^{15}N, respectively, r_{NH} is the amide bond length (1.02 Å), $\Delta\sigma$ is the chemical shift anisotropy (−160 p.p.m.) and R_{ex} is the chemical exchange contribution to R_2. J(ω) is the power spectral density function defining the reorientation of the N–H bond vector by stochastic (global) and intramolecular motions. Reduced spectral density mapping uses an average value of $J(\omega_H)$ for the linear combinations of $J(\omega_H + \omega_N)$, $J(\omega_H)$ and $J(\omega_H - \omega_N)$ leading to the values of J(0), $J(\omega_N)$ and $J(\omega_H)$ that are given by:

$$\sigma_{NH} = R_1(NOE - 1)\frac{\gamma_N}{\gamma_H}. \quad 4$$

$$J(\omega_H) = \frac{4\sigma_{NH}}{5d^2}. \quad 5$$

$$J(\omega_N) = \frac{[4R_1 - 5\sigma_{NH}]}{[3d^2 + 4c^2]}. \quad 6$$

$$J(0) = \frac{[6R_2 - 3R_1 - 2.72\sigma_{NH}]}{[3d^2 + 4c^2]}. \quad 7$$

This approach estimates the magnitude of the spectral density function at the given frequencies, making no assumptions about the form of the spectral density function or about the molecular behavior giving rise to the relaxation.

RESULTS AND DISCUSSION

NMR evidence for overlapping ssDNA- and p53TAD-binding sites on DBD F

The identification of minimal interacting domains for hRPA70 and p53 is a necessary step toward understanding the mechanism of p53–hRPA70 complex formation and disassociation. To test if $hRPA70_{1–168}$ and p53TAD are sufficient for complex formation, a ^1H–^{15}N HSQC titration experiment was performed on ^{15}N-labeled $hRPA70_{1–168}$. The amide ^1H–^{15}N HSQC resonances were monitored for a uniformly ^{15}N-labeled 0.60 mM sample of $hRPA70_{1–168}$ before and after the addition of unlabeled p53TAD to concentrations of 0.005, 0.01, 0.05, 0.10, 0.15, 0.30 and 0.60 mM. Chemical shift changes were observed after the addition of p53TAD to a concentration of 0.05 mM. Figure 2 shows a representative profile for one of the resonances most affected by binding. Figure 2 shows the resonances for A59 from overlapping ^1H–^{15}N HSQC spectra after the addition of p53TAD to concentrations of 0.0, 0.05, 0.10, 0.15, 0.30 and 0.60 mM. The starting position of the A59 resonance is indicated by the red box and crosshair. Arrows with p53TAD concentration values show the movement of the A59 resonance during the course of the titration. The small chemical shift changes observed between the last two points in the titration series indicates that the binding is approaching saturation. These results demonstrate that the p53TAD and

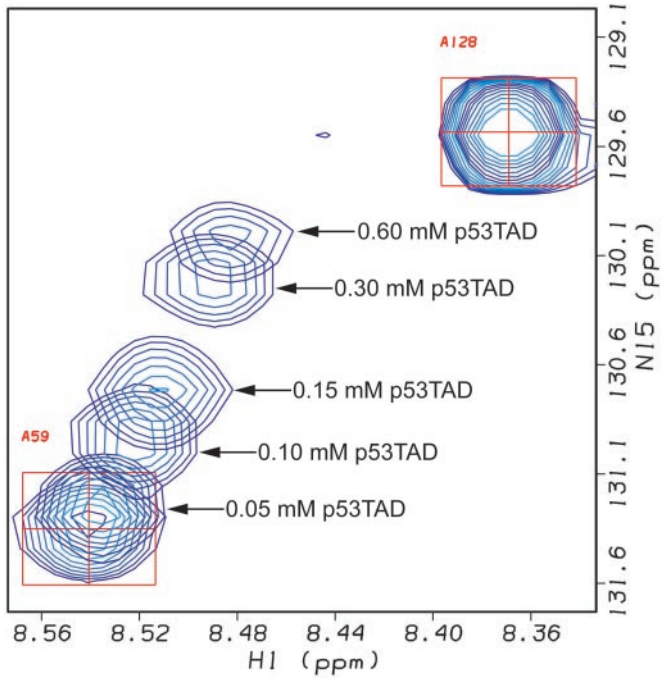

Figure 2. Overlapping ^1H–^{15}N HSQC spectra for A59 and A128 resonances obtained during titration between $hRPA70_{1–168}$ and p53TAD. A59 participates in binding while A128 does not. Spectra were collected at 298K.

hRAP70$_{1–168}$ fragments are sufficient for complex formation. Figure 2 also shows the resonance for A128, which experiences no chemical shift changes during the course of the titration.

The ability to track the chemical shift changes during the course of a titration permits assignment of the bound resonances based on the assumption of a minimal perturbation in the spectra. This process was used to make the amide ^{15}N and ^{1}H resonance assignments for the bound form of hRPA70$_{1–168}$. The amide ^{15}N and ^{1}H chemical shift changes observed between free hRPA70$_{1–168}$ and hRPA70$_{1–168}$ in the presence of 0.60 mM p53TAD were tabulated and averaged to identify the hRPA70$_{1–168}$ residues that are most affected by binding to p53TAD. The mean value for the averaged amide ^{15}N and ^{1}H chemical shift changes for residues M1-L122 of hRPA70$_{1–168}$ is 0.03 p.p.m. and the resolution for this measurement is 0.02 p.p.m. Chemical shift changes are not observed for hRPA70$_{1–168}$ residues that are C-terminal of L122. Small (<0.01 p.p.m.) or no chemical shift changes are observed for the majority of hRPA70$_{1–168}$ residues from M1-L122. HRPA70$_{1–168}$ residues with average chemical shift changes ⩾0.05 p.p.m. are G17, I30, I33, T35, G36, L45, S54, S55, F56, A59, T86, L87, R91, R92, V93, E98 and Y118.

Figure 3a shows a ribbon diagram of hRPA70 residues 1–114, which includes the DBD F and a short segment of the flexible linker. In Figure 3a, the positions of hRPA70$_{1–168}$ residues with chemical shift changes that are ⩾0.05 p.p.m. following the p53TAD titration are colored red. The side chains and labels are shown for the arginine and lysine residues that form the basic cleft. With the exception of G17 and E98, all of the hRPA70$_{1–168}$ residues that have chemical shift changes ⩾0.05 p.p.m. when bound to p53TAD are within 15 Å of the basic cleft. The chemical shift changes observed for the other basic cleft residues are as follows: R31 = 0.02 p.p.m., R41 = 0.03 p.p.m. and R43 = 0.04 p.p.m. Chemical shift values were not measured for K88 owing to resonance overlap.

In a previous study, an NMR titration strategy was used to identify a weak ssDNA-binding site that was also localized to the DBD F basic cleft (10). Figure 3b shows a ribbon diagram of DBD F with the hRPA70$_{1–168}$ residues that experienced the largest chemical shift changes after the addition of ssDNA colored red (10). These residues are T34, T35, R41, Y42, A59-L62, T86, D89, R91, V93 and Y118. Chemical shift changes were not observed for residues C-terminal of L122. In Figure 3b, all of the hRPA70$_{1–168}$ residues that have the largest chemical shift changes when bound to ssDNA are also within 15 Å of the basic cleft. A comparison of Figure 3a and b shows that p53TAD and ssDNA occupy overlapping but non-identical binding sites on DBD F. This conclusion is emphasized in Figure 3c, which shows the position of the hRPA70$_{1–168}$ residues that experience the largest chemical shift changes after the addition of either p53TAD or ssDNA. The position of these residues is shown relative to the linear sequence and secondary structure for hRPA70 residues 1–123.

The localization of the p53TAD (pI = 3.77) and ssDNA-binding sites to the DBD F basic cleft is expected since both molecules are negatively charged. The presence of overlapping p53TAD and ssDNA-binding sites on DBD F suggests that a competitive binding mechanism may regulate complex

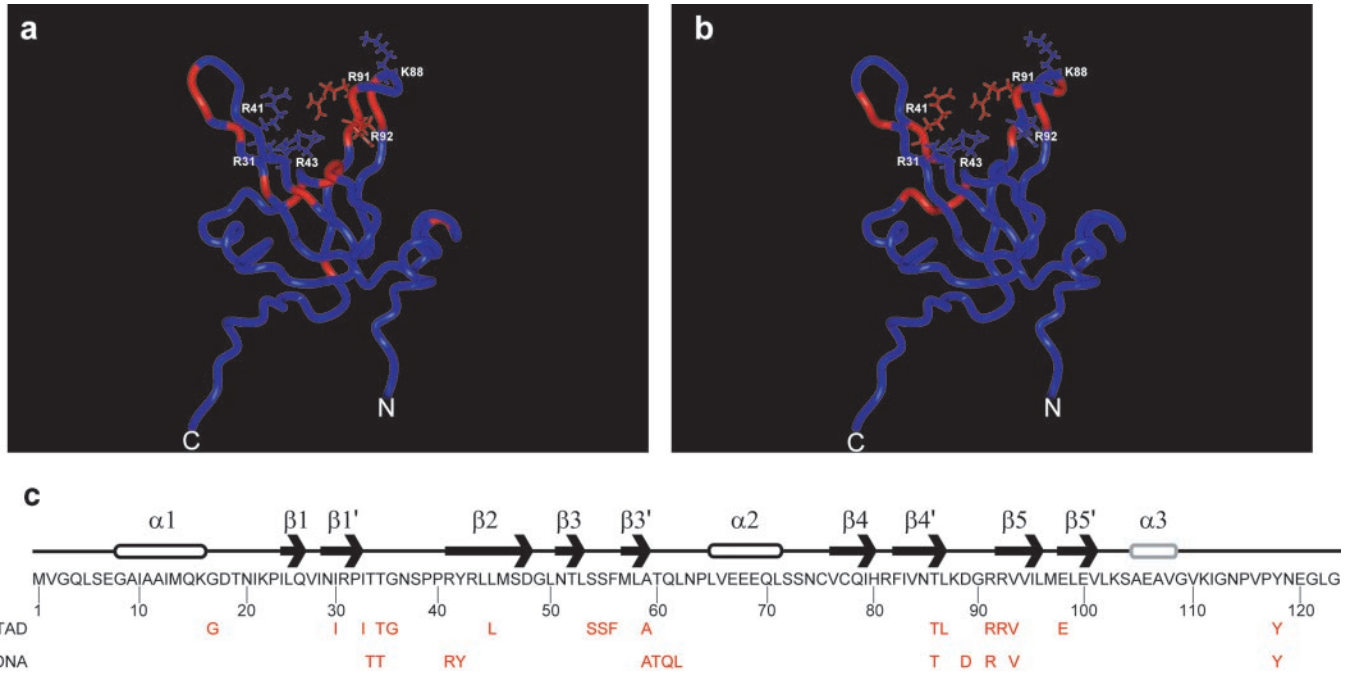

Figure 3. (**a**) Ribbon diagram of DBD F showing the position on the structure of residues with the largest chemical shift changes upon binding p53TAD colored red. (**b**) Ribbon diagram of DBD F showing the position on the structure of residues with the largest chemical shift changes upon binding ssDNA colored red. For (a) and (b), the N- and C-termini and the positively charged residues that form the DBD F basic cleft are labeled. (**c**) Schematic representation of the secondary structure and linear sequence for hRPA70 residues 1–123. β-Strands are labeled with arrows, α-helices are labeled with cylinders, and loop and coil regions are labeled with lines. The α3 helix is colored gray to reflect its reduced stability (9). Shown in red below the sequence are the hRPA70$_{1–168}$ residues with the largest chemical shift changes upon binding either p53TAD or ssDNA.

formation. This competition could modulate the disassociation of the hRAP70–p53 complex that occurs in response to DNA damage (21,24). While the affinity of p53TAD or ssDNA for DBD F has not been directly measured, an upper limit on the association constant can be inferred from the behavior of the resonance lines during the course of the titrations. For both titrations, the resonance lines in the DBD F ^{1}H–^{15}N HSQC spectra undergo chemical shifts that vary continuously with ligand concentration and the trajectories of these chemical shifts are linear and occur at the same rate for all residues that form the binding interfaces. When resonance lines undergo chemical shifts that vary continuously with ligand concentration, the bimolecular association constant, K_a, will be on the order of 10^5 (62). In addition, if the trajectories of the chemical shift changes are linear and occur at the same rate for all the residues that form the binding interface, then a single binding event is probable.

Identification of p53TAD residues important for binding hRPA70$_{1–168}$

^{1}H–^{15}N HSQC experiments were also performed on uniformly ^{15}N-labeled samples of p53TAD before and after the addition of increasing amounts of unlabeled hRPA70$_{1–168}$. The left panel of Figure 4 shows a selected region of the assigned ^{1}H–^{15}N HSQC spectrum of a 0.30 mM sample of p53TAD and the right panel shows the ^{1}H–^{15}N HSQC spectrum of the same sample after the addition of unlabeled hRPA70$_{1–168}$ to a concentration of 0.30 mM. In both spectra, the ^{1}H chemical shifts are plotted on the horizontal axis. The ^{15}N chemical shifts are plotted on the vertical axis of the spectrum on the right. The observed spectral changes that occurred after the addition of unlabeled hRPA70$_{1–168}$ are characterized by resonance intensity reductions and some small chemical shift changes. Owing to the interaction between hRPA70$_{1–168}$ and p53TAD, the resonances for residues 43–56 become so weak they can no longer be detected.

Resonance intensity measurements were made for 58 of the assigned non-proline residues in both of the Figure 4 spectra. An intensity ratio was calculated by dividing the resonance intensities of free p53TAD by the resonance intensities of p53TAD after the addition of hRPA70$_{1–168}$. Owing to the overlap of the D42 and M44 resonances and the W53 and F54 resonances these measurements represent an average value. The intensity ratios for the p53TAD resonances are plotted in Figure 5a. The $\log_{10}$ of the intensity ratio is plotted on the vertical axis and the residue type and number are plotted on the horizontal axis. Figure 5a shows that residues 39–59 have the largest resonance intensity changes in the presence of hRPA70$_{1–168}$ with residues 42–56 having intensity ratios that are >10. These data corroborate earlier affinity binding studies which suggested that residues 40–60 are essential for binding hRPA70 (21,47).

The residues adjacent to the 39–59 region of p53TAD showed some reduction in resonance intensities with residues 35–38 and 61–62 having mean intensity ratios of 3.5 ± 0.28 and 3.2 ± 0.19, respectively. A second region, including residues 19–28, had a mean intensity ratio of 3.5 ± 0.46. This region contains a transient amphipathic helix (43). Previous studies showed that mutations at residues 22 and 23 had minor effects on binding to hRPA70 (21). These previous results are consistent with the data in Figure 5a, which show that residues 19–28 contribute to binding hRPA70$_{1–168}$ but to a much smaller extent than residues 39–59. It was also previously reported

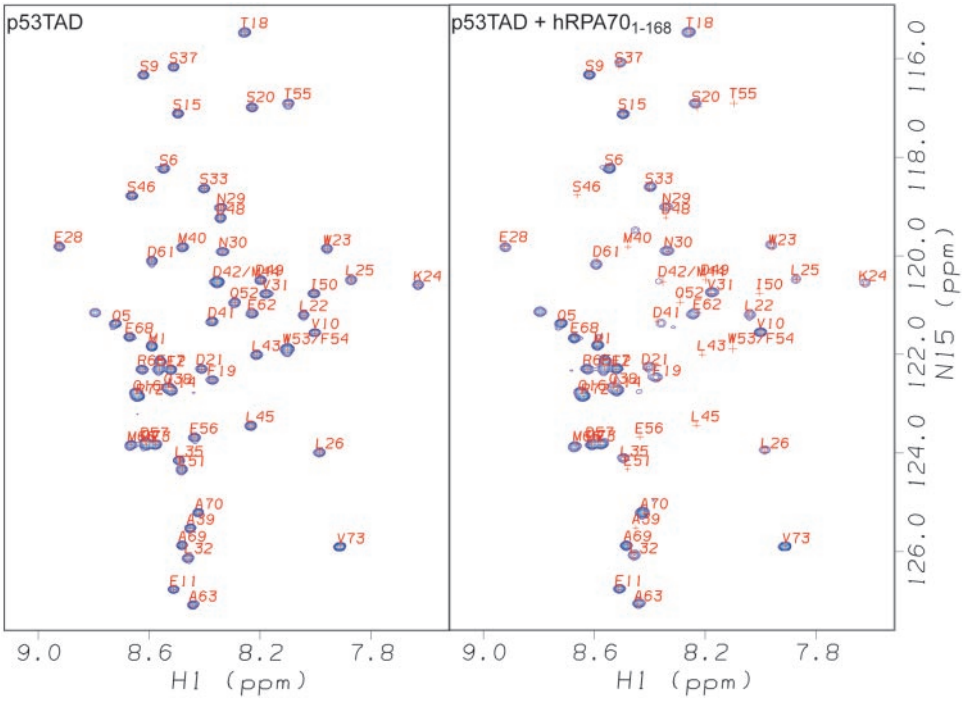

Figure 4. Selected regions of the assigned ^{1}H–^{15}N HSQC spectra of 0.30 mM uniformly ^{15}N-labeled p53TAD. The left panel shows p53TAD alone and the right panel shows p53TAD after the addition of unlabeled hRPA70$_{1–168}$ to a concentration of 0.30 mM. Both spectra were collected at 278K.

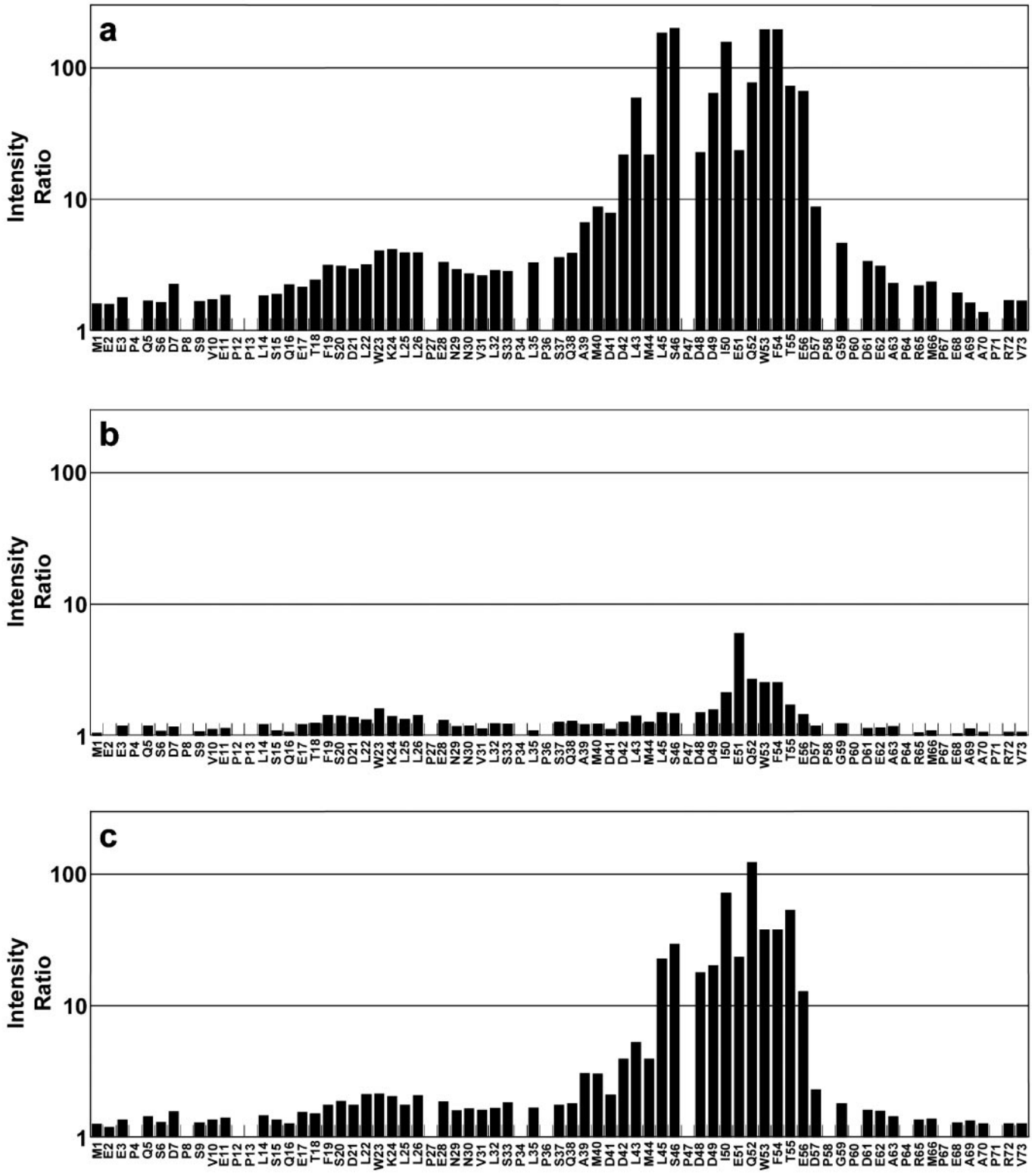

Figure 5. The calculated intensity ratios for p53TAD after the addition of (**a**) $hRPA70_{1–168}$, (**b**) R41E and (**c**) Y118A.

that two truncated versions of p53, consisting of residues 2–45 and 46–71, do not bind hRPA70 (47). This result is easily explained by the data in Figure 5a, which clearly show that both these truncated constructs eliminate residues that contribute strongly to the binding of $hRPA70_{1–168}$.

Importance of DBD F basic cleft residue R41 for complex formation

The results presented in Figures 2 and 3 demonstrate that p53TAD binds to the DBD F basic cleft. There are five aspartic acid residues and two glutamic acid residues in the p53TAD

sequence between residues 39 and 59. Of these seven negatively charged residues, five of them have an intensity ratio that is >10 in the binding experiment between p53TAD and $hRPA70_{1–168}$ as shown in Figure 5a. To examine the role of electrostatics on p53TAD–$hRPA70_{1–168}$ complex formation, an $hRPA70_{1–168}$ mutant that changed the basic cleft residue R41 to glutamic acid, R41E, was constructed and overexpressed. It is expected that the R41E mutation will significantly disrupt the electrostatic character of the basic cleft. It changes a positively charged residue into a negative one, which could interact with the other five positively charged residues in the basic cleft and could also be repulsive for the negatively charged residues of p53TAD. A $^{1}H–^{15}N$ HSQC spectrum was collected to verify that R41E was folded and no dramatic structural changes occurred relative to wild-type $hRPA70_{1–168}$ (data not shown). $^{1}H–^{15}N$ HSQC experiments were performed on uniformly ^{15}N-labeled samples of p53TAD before and after the addition of equimolar amounts of R41E. As expected, the R41E mutant binds weakly to p53TAD. The results in Figure 5b show small resonance intensity changes for all p53TAD residues after the addition of R41E. All of the intensity ratio values for the R41E experiment are below 2.0 except for residues I50-F54 which have a mean value of 3.3 ± 1.7. The lack of binding between p53TAD and R41E demonstrates the importance of electrostatics for p53TAD–$hRPA70_{1–168}$ complex formation.

Additional regions of $hRPA70_{1–168}$ involved in complex formation

$HRPA70_{1–168}$ contains the DBD F domain as well as a flexible linker between residues 105 and 168. Previous experiments have found one detectable NOE between the flexible linker and the DBD F (9). This NOE is between the flexible linker residue Y118 and the DBD F residue T52. In the titration experiments presented in Figures 2 and 3, T52 has an average chemical shift change of 0.02 p.p.m. and Y118 has an average chemical shift change of 0.06 p.p.m. A large chemical shift, such as 0.06 p.p.m. for Y118, is expected for residues involved in complex formation. To determine if Y118 is important for p53TAD–$hRPA70_{1–168}$ complex formation, an $hRPA70_{1–168}$ mutant that changed Y118 to alanine, Y118A, was overexpressed and purified. Similar to R41E, a $^{1}H–^{15}N$ HSQC spectrum was collected to verify that this mutant was folded and no dramatic structural changes occurred relative to wild-type $hRPA70_{1–168}$ (data not shown). To determine whether the elimination of Y118 significantly affected complex formation, a $^{1}H–^{15}N$ HSQC experiment was performed on an uniformly ^{15}N-labeled sample of p53TAD after the addition of an equimolar amount of Y118A. The intensity ratios were determined and plotted identically to the wild-type $hRPA70_{1–168}$ experiment and are shown in Figure 5c. The Y118A mutant binding is significantly diminished compared with wildtype. In wild-type, residues 42–56 have a mean intensity ratio of 95 ± 70 and in Y118A the mean intensity ratio is 35 ± 34, suggesting a 3-fold reduction in binding.

p53TAD resonance assignments and secondary chemical shifts

NMR resonance assignments correlate discrete signals observed in the NMR frequency spectrum of the protein with specific amino acid residues and they are very sensitive to changes in protein structure and dynamics. The observed NMR frequencies in the protein are referenced against some appropriate standard to generate a quantity called the chemical shift. The chemical shifts of $^{13}C^{\alpha}$, $^{13}C^{\beta}$, ^{13}CO and $^{1}H^{\alpha}$ nuclei can be used to make a rapid, semi-quantitative identification of protein secondary structure (63–66). This method has been widely applied to IUPs, such as p53TAD, with some general observations worth noting (67,68). Many IUPs do not have regions of stable secondary structure in the absence of binding partners and are rapidly interconverting between an unspecified number of structures. When the interconversion rate is fast on the NMR timescale [$\geqslant 10^{4}$ s^{-1} (69)] the chemical shift represents a population weighted average of the different structures that make up the ensemble. In this case, the secondary chemical shift ($\Delta\delta$), which is the difference between observed chemical shift and some appropriate residue specific random coil chemical shift standard, can be used to provide an estimate of the fraction of structures that are in a helical or β-strand conformation. A less general observation from the chemical shift analysis of IUPs is that $\Delta\delta$ values can switch from positive to negative several times over a short stretch of the polypeptide sequence (70–72). A clear structural interpretation for this behavior has not been proposed. In addition, the $\Delta\delta$ values for $^{13}C^{\alpha}$, $^{13}C^{\beta}$, ^{13}CO and $^{1}H^{\alpha}$ nuclei do not always correlate for IUPs, making the unambiguous identification of transient secondary structure challenging (73).

Resonance assignments were made for the $^{13}C^{\alpha}$, $^{13}C^{\beta}$, ^{13}CO and $^{1}H^{\alpha}$ nuclei as well as the amide ^{15}N and ^{1}H nuclei of p53TAD. The $\Delta\delta$ values were determined for the $^{13}C^{\alpha}$, $^{13}C^{\beta}$, ^{13}CO and $^{1}H^{\alpha}$ nuclei of p53TAD and are plotted in Figure 6a–d. The residue specific random coil chemical shift standard used to calculate the $\Delta\delta$ values in Figure 6 was developed by Wishart *et al*. (74) and is based on chemical shift measurements for short peptides dissolved in 1 M urea (pH 5.0). For $^{13}C^{\alpha}$ and ^{13}CO nuclei, a positive $\Delta\delta$ value indicates a preference for α-helical structure and a negative $\Delta\delta$ value indicates a preference for β-strand structure (63–65). The trend is reversed for $^{1}H^{\alpha}$ nuclei. For $^{13}C^{\beta}$ nuclei, positive $\Delta\delta$ values indicate the presence of β-strand structure, $\Delta\delta$ values near zero indicate the presence of α-helical structure and negative $\Delta\delta$ values indicate the presence of structures with positive ϕ and ψ angles (64).

It is well established that p53TAD residues 18–24 form an amphipathic α-helix when bound to the MDM2 oncoprotein (75). It is also well established that unbound IUPs, such as p53TAD, will often show some preference for the secondary structure that is observed when they form a protein complex (76). In keeping with this principle, the $^{1}H^{\alpha}$ $\Delta\delta$ values plotted in Figure 6d suggest the presence of a transient α-helix spanning residues 18–24. This result confirms earlier work that reported a transient α-helix between residues 18 and 26 using $^{1}H^{\alpha}$ chemical shifts as well as three bond coupling constants (43). Interestingly, the $\Delta\delta$ values for the ^{13}CO and $^{13}C^{\alpha}$ nuclei do not show a strong preference for helical structure for residues 18–24 and the trend observed for the $^{13}C^{\beta}$ $\Delta\delta$ values suggest a mixture of α-helix and structures with positive ϕ and ψ angles for residues 13–28 (64).

The $^{13}C^{\alpha}$ and ^{13}CO $\Delta\delta$ values suggest that the DBD F binding site (residues 39–59) contains a mixture of α-helical, β-strand and random coil structures. For both $^{13}C^{\alpha}$ and ^{13}CO,

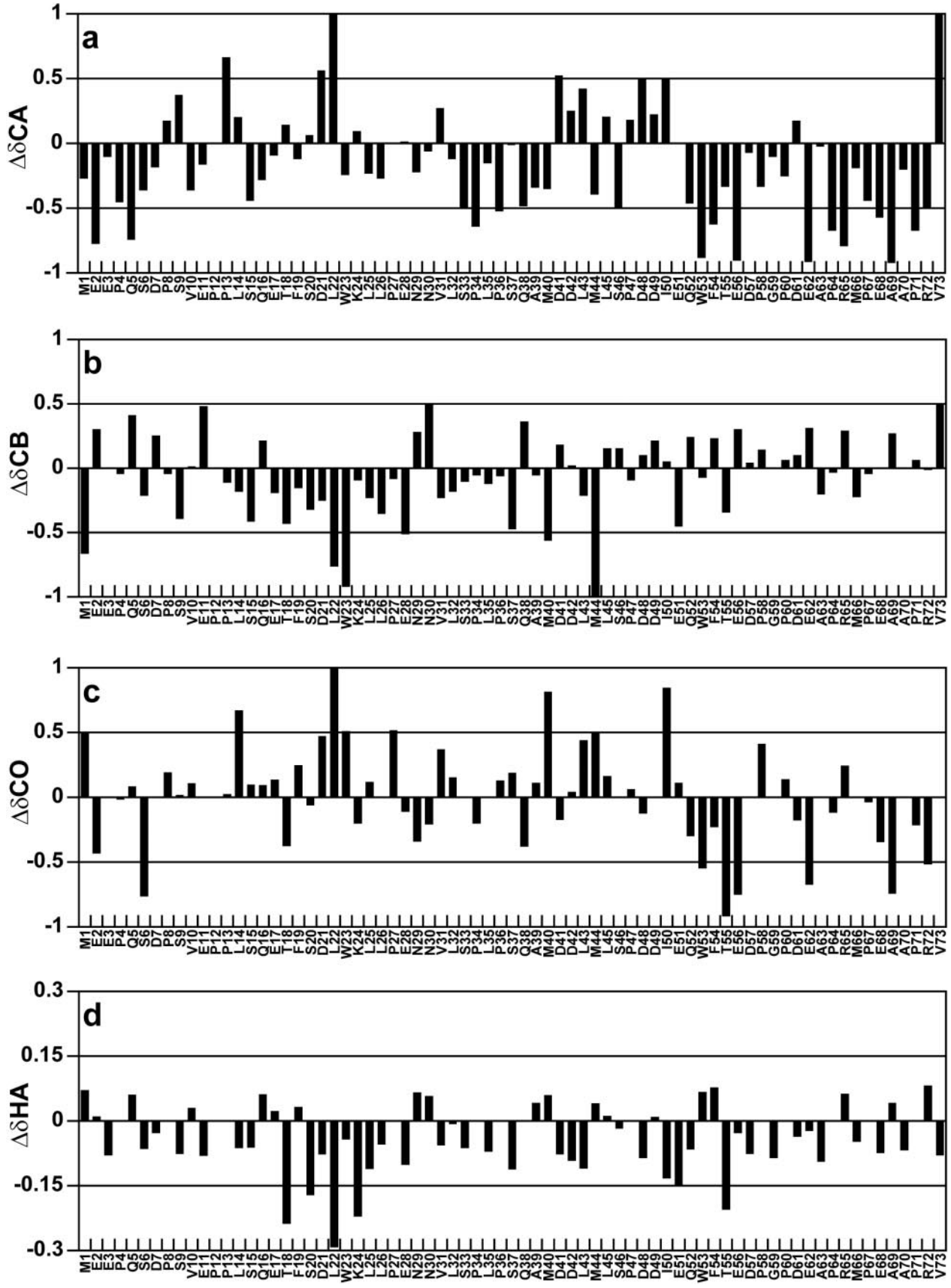

Figure 6. Plots showing secondary chemical shifts for p53TAD based on resonance assignments obtained at 298K. The random coil chemical shift standard used in the analysis was developed by Wishart *et al.* (74). (**a**) Plot of $^{13}C^{\alpha}$ Δδ values, (**b**) plot of $^{13}C^{\beta}$ Δδ values, (**c**) plot of ^{13}CO Δδ values and (**d**) plot of $^{1}H^{\alpha}$ Δδ values.

a transition from positive to negative Δδ values is observed between I50 and Q52. The ^{1}H–^{15}N HSQC resonances for E51 and Q52 are the first to disappear during the titration of ^{15}N-labeled p53TAD, suggesting that these residues are strongly interacting with the DBD F basic cleft (data not shown). The data presented in Figure 6 show some evidence for transient α-helical and β-strand secondary structure in the DBD F binding region of p53TAD. To determine whether this transient secondary structure is stabilized upon binding, HNCACB experiments were performed on p53TAD in the presence of increasing amounts of unlabeled $hRPA70_{1–168}$. The results from these experiments showed no $^{13}C^{\alpha}$ and $^{13}C^{\beta}$ chemical shift changes before the resonances became too weak to detect (data not shown).

Relaxation measurements and reduced spectral density mapping for free and bound p53TAD

NMR relaxation measurements can be used to identify the residue specific changes in rotational diffusion that occur when two proteins form a complex. A standard suite of ^{15}N relaxation experiments was collected on free p53TAD and the p53TAD–$hRPA70_{1–168}$ complex at a stoichiometry of 4:1. At this stoichiometry, the majority of ^{1}H–^{15}N HSQC resonances are still observed for p53TAD residues in the DBD F binding region (data not shown). Table 1 shows the mean values of R_1, R_2, $R_{1\rho}$ and the ^{1}H–^{15}N NOE (NHNOE) for free and bound p53TAD. These four relaxation measurements vary systematically with the rate of rotational diffusion and provide a very sensitive way to discriminate between folded and unfolded regions in a protein. For instance, the mean values of R_1, R_2, $R_{1\rho}$ and the NHNOE for free p53TAD are consistent with values expected for an intrinsically unstructured protein (67). R_2 is also sensitive to slower motions, like protein folding or chemical exchange.

Figure 7a–d shows plots of the ^{15}N relaxation rates R_1, R_2, $R_{1\rho}$ and the NHNOE for free and bound p53TAD using open and closed circles, respectively. Figure 7b and c show that large changes in R_2 and $R_{1\rho}$ are observed for several residues in the binding region when free and bound p53TAD are compared. Observing differences between these two relaxation rates is one of the first steps in discriminating between changes in relaxation that are induced by changes in rotational diffusion versus slower processes like protein folding or chemical exchange. Figure 7b and c also shows that no significant changes in R_2 and $R_{1\rho}$ occur for residues 1–35 and 62–73 when free and bound p53TAD are compared. This means that residues 1–35 and 62–73 remain unfolded and do not participate in complex formation.

For residues with a large chemical exchange contribution to relaxation, R_2 should be greater than $R_{1\rho}$ (77). This is the case for residues 42, 45, 48, 50 and 55. Other residues in the binding interface that have similar values of R_2 and $R_{1\rho}$ include 46, 49, 53/54, 56 and 57. It was not possible to accurately measure R_2 and $R_{1\rho}$ for residues 51 and 52 at the 4:1 stoichiometry. We hypothesize that the pattern of large R_2 and $R_{1\rho}$ values observed for residues 42, 45, 48 and 50, represent points of contact between these residues and DBD F. If this is the case, then the large R_2 and $R_{1\rho}$ values observed for every third residue (42, 45 and 48) may represent the formation of two turns of a 3^{10} helix. This conclusion is supported by the small helical Δδ values observed for residues 42, 45 and 48 (see Figure 6a). The pattern of R_2 and $R_{1\rho}$ values observed for residues C-terminal of 48 suggests that binding occurs in an extended conformation.

The relaxation data for free and bound p53TAD was analyzed using the reduced spectral density mapping approach of Farrow *et al*. (78). Reduced spectral density mapping is useful for estimating the timescale of molecular motions occurring at three different frequencies, the zero frequency, the ^{15}N resonance frequency and the ^{1}H resonance frequency. The reduced spectral density function at zero frequency, $J(0)$, is correlated with global rotational tumbling, the reduced spectral density function at the ^{15}N resonance frequency, $J(\omega_N)$, is correlated with faster segmental motions and the reduced spectral density function at the ^{1}H resonance frequency, $J(\omega_H)$, is correlated with even faster internal motions like bond vector fluctuations. The statistics summarizing the reduced spectral density mapping values at 0, ω_N and ω_H frequencies for free and bound p53TAD are listed in Table 1. Figure 8a–c shows plots of $J(0)$, $J(\omega_N)$ and $J(\omega_H)$ for free and bound p53TAD using open and closed circles, respectively. The $J(0)$ values plotted in Figure 8a were calculated using the R_2 values from Figure 7b and, therefore, contain contributions from chemical exchange. $J(0)$ values were also calculated substituting the $R_{1\rho}$ values in Figure 7c for R_2 (data not shown). $J(0)$ values calculated using $R_{1\rho}$ are 20–30% smaller for residues 42, 45, 48 and 50 than those calculated using R_2. The differences in $J(0)$ can be used to estimate the exchange term, R_{ex} (58). For residue 50, the value of $J(0)$ calculated using R_2 is 8.78 ns and the value calculated using $R_{1\rho}$ is 6.07 ns. This difference of 2.71 ns corresponds to an R_{ex} value of 8.36 s^{-1}. Residues 42, 45 and 48 have R_{ex} values in the range of 1–10 s^{-1} (data not shown). Values of R_{ex} in the range of 1–10 s^{-1} have been observed for protein folding intermediates and conformational fluctuations that occur on the timescale of protein folding (79–81). The large R_{ex} values observed for residues 42, 45, 48 and 50 suggest that the DBD F binding region of p53TAD undergoes a folding transition upon binding.

Table 1. Statistics for relaxation and reduced spectral density mapping data

	p53TAD	p53TAD + $hRPA70_{1–168}$
R_1	1.74 ± 0.22	1.69 ± 0.23
R_2	3.16 ± 0.56	4.13 ± 2.21
$R_{1\rho}$	3.81 ± 0.66	4.55 ± 1.45
NHNOE	−0.64 ± 0.95	−0.51 ± 0.75
$J(0)$	1.61 ± 0.36	2.33 ± 1.62
$J(\omega_N)$	0.74 ± 0.15	0.72 ± 0.14
$J(\omega_H)$	0.064 ± 0.037	0.058 ± 0.029

CONCLUSIONS

Over the past decade, significant controversy has arisen concerning the functional significance of the p53–hRPA70 interaction. *In vitro* binding studies have shown that p53 and hRPA70 form a complex that can inhibit p53 from site-specific DNA binding and transcriptional activation (22,24). This inhibition is relieved in the presence of ssDNA (24). It is also known that hRPA70 has a higher affinity for ssDNA than for p53 and the addition of ssDNA causes the release of p53 from a preformed p53–hRPA70 complex (19,24,82). Based on

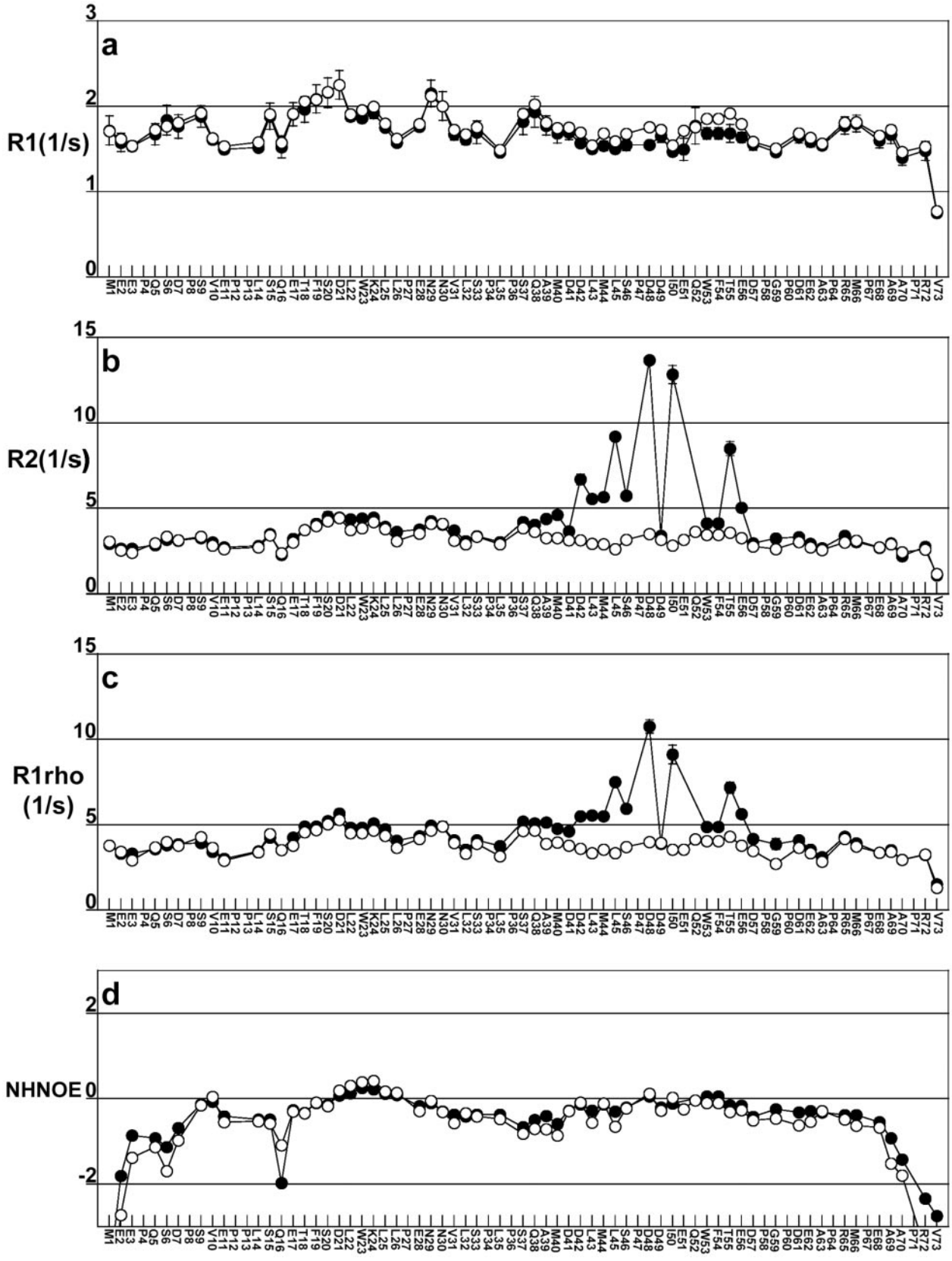

Figure 7. Plots showing relaxation data for p53TAD (open circles) and p53TAD plus unlabeled hRPA70$_{1-168}$ (closed circles). (**a**) Plot of the longitudinal relaxation rates, R_1, labeled R1; (**b**) plot of the transverse relaxation rates, R_2, labeled R2; (**c**) plot of the rotating frame relaxation rates, $R_{1\rho}$, labeled R1rho; and (**d**) plot of the ^{1}H–^{15}N NOE labeled NHNOE. Error bars are shown for the noisiest datasets, which in all cases is for bound p53TAD. For most of the p53TAD residues, error values are smaller than the data markers.

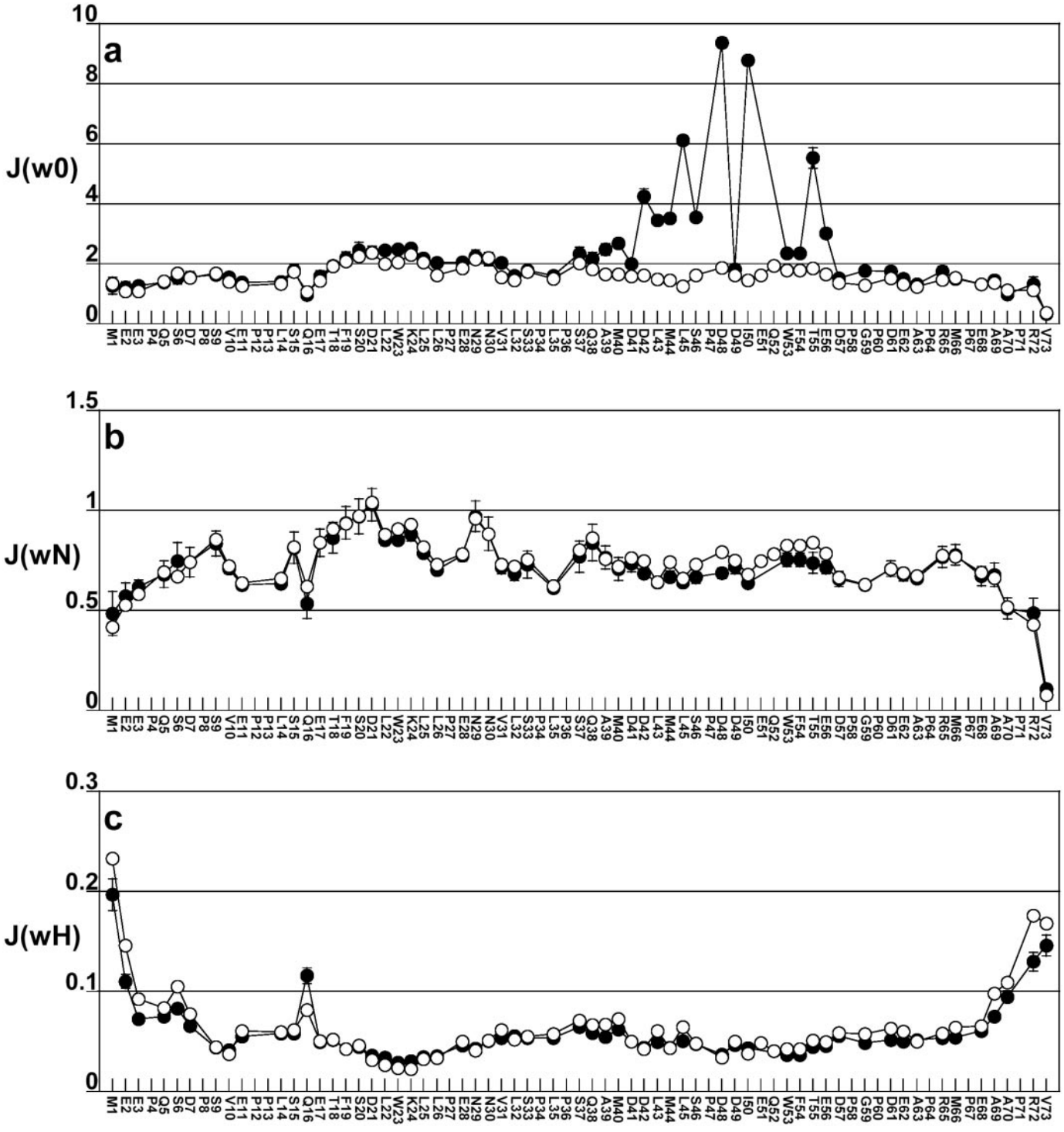

Figure 8. Plots of reduced spectral density mapping data for p53TAD (open circles) and p53TAD plus unlabeled hRPA70$_{1–168}$ (closed circles). (**a**) Plot of the spectral density at zero frequency, $J(0)$, labeled J(w0); (**b**) plot of the spectral density at the ^{15}N frequency, $J(\omega_N)$, labeled J(wN); and (**c**) plot of the spectral density at the ^{1}H frequency, $J(\omega_H)$, labeled J(wH). Error bars are shown for the noisiest datasets, which in all cases is for bound p53TAD. For most of the p53TAD residues, error values are smaller than the data markers.

these observations, Prives and co-workers (24,27) have suggested that the p53–hRPA70 complex provides a reservoir of p53 that is immediately available to control the transcription of DNA repair, apoptosis and growth arrest genes when released from hRPA70. This hypothesis is consistent with the observation that hRPA isolated from UV-treated cells does not bind p53, suggesting that complex formation is regulated by the presence of DNA damage and perhaps the phosphorylation of hRPA32 (21,83,84). According to Abramova *et al.* (21), the p53–hRPA70 interaction plays a role in linking

p53 to DNA damage. They observed that UV radiation disrupts the p53–hRPA70 interaction in a dose- and time-dependent manner. Furthermore, the disruption of p53–hRPA70 binding was correlated with the ability of damaged cells to perform global genomic repair. These results suggest that after UV irradiation the hRPA heterotrimer participates in nucleotide excision repair and simultaneously releases the bound p53 (21). This idea is consistent with the role of hRPA70 in the early stages of nucleotide excision repair (85). hRPA70 binds to the ssDNA exposed by open complex formation using DBD A and DBD B and may bind directly to the damaged site using DBD C (17,18). At some point during this recognition process p53 will disassociate from hRPA70.

In this report we present evidence that p53TAD and $hRPA70_{1–168}$ are sufficient for complex formation. Further, results are presented which show that p53TAD binds to the DBD F basic cleft. In summation, the results of this paper provide support for the hypothesis that p53TAD and ssDNA compete for an overlapping binding site on the DBD F basic cleft. NMR experiments in this paper demonstrate the importance of electrostatics for the binding of p53TAD to the basic cleft. A single mutation in a basic cleft residue, R41E, is sufficient for eliminating binding. Further, a mutation in the $hRPA70_{1–168}$ linker, Y118A, has diminished binding. A recent study in this laboratory has proposed a new model for the DBD F structure that incorporates the Y118–T52 interaction (K.E. Olson, P.D. Vise, P. Narayanaswami, D.F. Lowry, M.S. Wold and G.W. Daughdrill, manuscript in preparation). In this model, hRPA70 linker residues between Y118 and A128 are in a position to occlude the basic cleft and possibly provide an additional layer of regulation for interactions with the basic cleft. $^{1}H–^{15}N$ HSQC experiments were performed demonstrating that the region between p53TAD residues 39 and 59 had the largest change in resonance intensity and are the residues responsible for forming the binding interface with $hRPA70_{1–168}$. No differences were seen in the secondary structure of p53TAD in the presence and absence of $hRPA70_{1–168}$. However, a p53TAD-binding site identified by NMR analysis in this paper was shown to have some residual α-helical and β-strand structure. This residual secondary structure had not been identified in earlier NMR studies.

NMR titrations are a very powerful tool for the analysis of protein–protein interactions. In addition to identifying the binding interface, NMR titrations can provide information about the kinetics and thermodynamics of the interaction (62). When resonances change their position, similar to those observed in the HSQC spectrum of ^{15}N-labeled $hRPA70_{1–168}$ after the addition of unlabeled p53TAD, the rate of exchange between the free and bound structures is fast with an exchange rate constant, k, on the order of 10^{3}–10^{4} s^{-1} (69). When resonances lose intensity with no apparent chemical shift changes, similar to those observed for ^{15}N-labeled p53TAD after the addition of unlabeled $hRPA70_{1–168}$, the rate of exchange between the free and bound structures is intermediate with a value for k on the order of 10^{2}–10^{3} s^{-1}. These well-established relationships between resonance behavior and rates of exchange facilitate an explanation for the differences in the NMR titration results presented in Figures 2 and 4. Because the same proteins are binding one another, the same type of chemical shift changes in the HSQC resonances should be observed regardless of which protein is ^{15}N-labeled. There must be some additional process that is slowing down the exchange rate between the free and the bound forms of p53TAD when compared with $hRPA70_{1–168}$. One obvious process that would slow down complex formation is the folding of p53TAD. The effect of this folding would only be observed when the HSQC resonances of ^{15}N-labeled p53TAD are monitored. It is unclear as to exactly what structure of p53TAD is formed when it binds to DBD F. Further, folding could simply describe a rigidly held form of p53TAD that is an extended conformation. Using NMR relaxation measurements and reduced spectral density mapping, we have identified a large chemical exchange contribution to the ^{15}N transverse relaxation rates (R_2) of p53TAD residues that form the binding interface with $hRPA70_{1–168}$. Based on the argument presented above it is likely that this chemical exchange contribution to ^{15}N transverse relaxation is due to the folding of p53TAD.

Since p53TAD is highly acidic (pI = 3.77) and DBD F contains a positively charged cleft with five arginines and one lysine, it is reasonable to expect that electrostatics will play a prominent role in p53TAD–DBD F complex formation and that the acidic residues in p53TAD will have a favorable electrostatic interaction with the basic cleft. This hypothesis is strongly supported by the data presented in Figures 3 and 5. Based on the distribution of negatively charged amino acid pairs in the primary sequence of p53TAD (see Figure 1), it is possible that this favorable electrostatic interaction occurs between one pair of negatively charged residues in p53TAD and the positively charged DBD F basic cleft. This will result in the formation of an encounter complex that can then undergo a structural rearrangement to optimize the stability of the complex. This hypothesis assumes that the formation of the encounter complex represents a dynamically bound state for p53TAD that allows the protein to 'check the binding site' using the peptide segments that are adjacent to the pair of negative residues. If favorable van der Waals and hydrogen bonding interactions are available, then a tighter complex will be formed. If no favorable interactions are encountered then a new binding site will be 'checked' at the next pair of negative residues. If the energetics of encounter complex formation are dominated by ionic interactions between the negatively charged pairs and the basic cleft, then all of the encounter complexes will have similar affinities.

A simplified model based on the overlapping p53TAD and ssDNA-binding sites identified on DBD F is illustrated in Figure 9. We hypothesize that before DNA damage is detected, p53 is bound to hRPA70. Data presented in this report provide strong evidence for the interaction between p53TAD and DBD F that is shown in Figure 9. The interaction between the C-terminal regulatory domain of p53 and the DBD C is more speculative. After DNA damage is detected, DBD A and B will bind with high affinity to the ssDNA that is exposed during formation of the open complex. When this occurs, the flexibility and length of the linker will determine the orientation and mobility of DBD F relative to ssDNA. According to our model, this linkage effect will increase the affinity of DBD F for ssDNA by increasing the local concentration of ssDNA. The increased affinity between DBD F and ssDNA will result in the disassociation of p53 from hRPA70. It is unclear what p53 does after it is released from hRPA70. It is tantalizing to speculate that p53 will activate the transcription of apoptosis

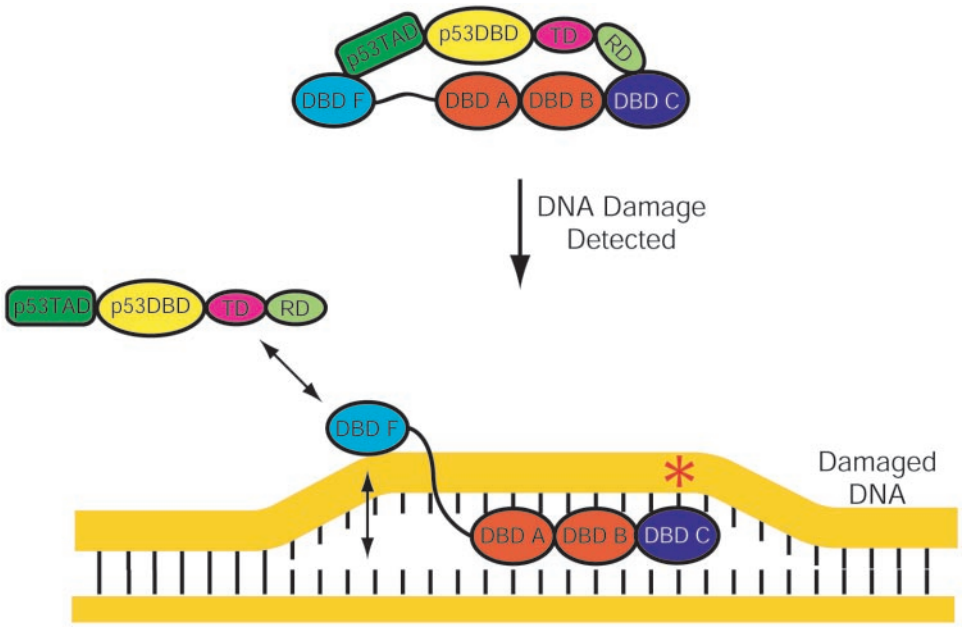

Figure 9. Model for p53–hRPA70 disassociation. Prior to DNA damage p53 and hRPA70 form a complex. When DNA damage occurs, hRPA70 binds and stabilizes the open complex. When this occurs DBD A and B will bind the undamaged strand. This will enhance the weak ssDNA-binding affinity of DBD F presumably to the point where p53 is released.

and growth arrest genes to amplify the cellular response to DNA damage.

ACKNOWLEDGEMENTS

We gratefully acknowledge Dr Lee Fortunato for the gift of the p53 cDNA and helpful discussions during the preparation of this manuscript. This publication was made possible by ACS Grant IRG7700323 and NIH Grant P20 RR 16448 from the COBRE Program of the National Center for Research Resources. Its contents are solely the responsibility of the authors and do not necessarily represent the official views of ACS or NIH. The NMR data presented in this publication was collected at the University of Idaho Structural Biology Core Facility. This facility is funded by NIH Grant P20 RR 16448 from the COBRE Program and P20 RR 16454-02 from the BRIN program. Both programs are part of the National Center for Research Resources. Funding to pay the Open Access publication charges for this article was provided by NIH Grant P20 RR 16448.

Conflict of interest statement. None declared.

REFERENCES

1. Friedberg,E.C. (1997) *Correcting the Blueprint of Life: An Historical Account of the Discovery of DNA Repair Mechanisms*. Cold Spring Harbor Laboratory Press, Cold Spring Harbor, NY, pp. 17–19, 91–96.
2. Friedberg,E.C., Walker,G.C. and Siede,W. (1995) *DNA Repair and Mutagenesis*. ASM Press, Washington, DC, pp. 1–29, 1–92.
3. Lindahl,T., Karran,P. and Wood,R.D. (1997) DNA excision repair pathways. *Curr. Opin. Genet. Dev.*, **7**, 158–169.
4. Wallace,S.S., Van Houten,B. and Kow,Y.W. (1994) *DNA Damage: Effect on DNA Structure and Protein Recognition*. Annals of the New York Academy of Sciences, pp. 92–105.
5. Wold,M.S. (1997) Replication protein A: a heterotrimeric, single-stranded DNA-binding protein required for eukaryotic DNA metabolism. *Annu. Rev. Biochem.*, **66**, 61–92.
6. He,Z., Henricksen,L.A., Wold,M.S. and Ingles,C.J. (1995) RPA involvement in the damage-recognition and incision steps of nucleotide excision repair. *Nature*, **374**, 566–569.
7. Wold,M.S. and Kelly,T. (1988) Purification and characterization of replication protein A, a cellular protein required for *in vitro* replication of simian virus 40 DNA. *Proc. Natl Acad. Sci. USA*, **85**, 2523–2527.
8. Fairman,M.P. and Stillman,B. (1988) Cellular factors required for multiple stages of SV40 DNA replication *in vitro*. *EMBO J.*, **7**, 1211–1218.
9. Jacobs,D.M., Lipton,A.S., Isern,N.G., Daughdrill,G.W., Lowry,D.F., Gomes,X. and Wold,M.S. (1999) Human replication protein A: global fold of the N-terminal RPA-70 domain reveals a basic cleft and flexible C-terminal linker. *J. Biomol. NMR*, **14**, 321–331.
10. Daughdrill,G.W., Ackerman,J., Isern,N.G., Botuyan,M.V., Arrowsmith,C., Wold,M.S. and Lowry,D.F. (2001) The weak interdomain coupling observed in the 70 kDa subunit of human replication protein A is unaffected by ssDNA binding. *Nucleic Acids Res.*, **29**, 3270–3276.
11. Braun,K.A., Lao,Y., He,Z., Ingles,C.J. and Wold,M.S. (1997) Role of protein–protein interactions in the function of replication protein A (RPA): RPA modulates the activity of DNA polymerase alpha by multiple mechanisms. *Biochemistry*, **36**, 8443–8454.
12. Gomes,X.V. and Wold,M.S. (1995) Structural analysis of human replication protein A. Mapping functional domains of the 70-kDa subunit. *J. Biol. Chem.*, **270**, 4534–4543.
13. He,Z., Brinton,B.T., Greenblatt,J., Hassell,J.A. and Ingles,C.J. (1993) The transactivator proteins VP16 and GAL4 bind replication factor A. *Cell*, **73**, 1223–1232.
14. Oakley,G.G., Patrick,S.M., Yao,J., Carty,M.P., Turchi,J.J. and Dixon,K. (2003) RPA phosphorylation in mitosis alters DNA binding and protein–protein interactions. *Biochemistry*, **42**, 3255–3264.
15. Bochkarev,A., Pfuetzner,R.A., Edwards,A.M. and Frappier,L. (1997) Structure of the single-stranded-DNA-binding domain of replication protein A bound to DNA. *Nature*, **385**, 176–181.
16. Lin,Y.L., Chen,C., Keshav,K.F., Winchester,E. and Dutta,A. (1996) Dissection of functional domains of the human DNA replication protein complex replication protein A. *J. Biol. Chem.*, **271**, 17190–17198.

17. Lao,Y., Gomes,X.V., Ren,Y., Taylor,J.S. and Wold,M.S. (2000) Replication protein A interactions with DNA. III. Molecular basis of recognition of damaged DNA. *Biochemistry*, **39**, 850–859.
18. Lao,Y., Lee,C.G. and Wold,M.S. (1999) Replication protein A interactions with DNA. 2. Characterization of double-stranded DNA-binding/helix-destabilization activities and the role of the zinc-finger domain in DNA interactions. *Biochemistry*, **38**, 3974–3984.
19. Walther,A.P., Gomes,X.V., Lao,Y., Lee,C.G. and Wold,M.S. (1999) Replication protein A interactions with DNA. 1. Functions of the DNA-binding and zinc-finger domains of the 70-kDa subunit. *Biochemistry*, **38**, 3963–3973.
20. Iftode,C., Daniely,Y. and Borowiec,J.A. (1999) Replication protein A (RPA): the eukaryotic SSB. *Crit. Rev. Biochem. Mol. Biol.*, **34**, 141–180.
21. Abramova,N.A., Russell,J., Botchan,M. and Li,R. (1997) Interaction between replication protein A and p53 is disrupted after UV damage in a DNA repair-dependent manner. *Proc. Natl Acad. Sci. USA*, **94**, 7186–7191.
22. Dutta,A., Ruppert,J.M., Aster,J.C. and Winchester,E. (1993) Inhibition of DNA replication factor RPA by p53. *Nature*, **365**, 79–82.
23. Li,R. and Botchan,M.R. (1993) The acidic transcriptional activation domains of VP16 and p53 bind the cellular replication protein A and stimulate *in vitro* BPV-1 DNA replication. *Cell*, **73**, 1207–1221.
24. Miller,S.D., Moses,K., Jayaraman,L. and Prives,C. (1997) Complex formation between p53 and replication protein A inhibits the sequence-specific DNA binding of p53 and is regulated by single-stranded DNA. *Mol. Cell. Biol.*, **17**, 2194–2201.
25. Bargonetti,J. and Manfredi,J.J. (2002) Multiple roles of the tumor suppressor p53. *Curr. Opin. Oncol.*, **14**, 86–91.
26. Levine,A.J. (1997) p53, the cellular gatekeeper for growth and division. *Cell*, **88**, 323–331.
27. Haupt,Y., Robles,A.I., Prives,C. and Rotter,V. (2002) Deconstruction of p53 functions and regulation. *Oncogene*, **21**, 8223–8231.
28. Shaulian,E., Schreiber,M., Piu,F., Beeche,M., Wagner,E.F. and Karin,M. (2000) The mammalian UV response: c-Jun induction is required for exit from p53-imposed growth arrest. *Cell*, **103**, 897–907.
29. Zhou,J., Ahn,J., Wilson,S.H. and Prives,C. (2001) A role for p53 in base excision repair. *EMBO J.*, **20**, 914–923.
30. Zhou,J. and Prives,C. (2003) Replication of damaged DNA *in vitro* is blocked by p53. *Nucleic Acids Res.*, **31**, 3881–3892.
31. Liu,W.L., Midgley,C., Stephen,C., Saville,M. and Lane,D.P. (2001) Biological significance of a small highly conserved region in the N terminus of the p53 tumour suppressor protein. *J. Mol. Biol.*, **313**, 711–731.
32. Walker,K.K. and Levine,A.J. (1996) Identification of a novel p53 functional domain that is necessary for efficient growth suppression. *Proc. Natl Acad. Sci. USA*, **93**, 15335–15340.
33. Hollstein,M., Rice,K., Greenblatt,M.S., Soussi,T., Fuchs,R., Sorlie,T., Hovig,E., Smith-Sorensen,B., Montesano,R. and Harris,C.C. (1994) Database of p53 gene somatic mutations in human tumors and cell lines. *Nucleic Acids Res.*, **22**, 3551–3555.
34. Hollstein,M., Shomer,B., Greenblatt,M., Soussi,T., Hovig,E., Montesano,R. and Harris,C.C. (1996) Somatic point mutations in the p53 gene of human tumors and cell lines: updated compilation. *Nucleic Acids Res.*, **24**, 141–146.
35. Shieh,S.Y., Taya,Y. and Prives,C. (1999) DNA damage-inducible phosphorylation of p53 at N-terminal sites including a novel site, Ser20, requires tetramerization. *EMBO J.*, **18**, 1815–1823.
36. Lee,W., Harvey,T.S., Yin,Y., Yau,P., Litchfield,D. and Arrowsmith,C.H. (1994) Solution structure of the tetrameric minimum transforming domain of p53. *Nature Struct. Biol.*, **1**, 877–890.
37. Arrowsmith,C.H. (1999) Structure and function in the p53 family. *Cell Death Differ.*, **6**, 1169–1173.
38. Arrowsmith,C.H. and Morin,P. (1996) New insights into p53 function from structural studies. *Oncogene*, **12**, 1379–1385.
39. Zhao,K., Chai,X., Johnston,K., Clements,A. and Marmorstein,R. (2001) Crystal structure of the mouse p53 core DNA-binding domain at 2.7 Å resolution. *J. Biol. Chem.*, **276**, 12120–12127.
40. Cho,Y., Gorina,S., Jeffrey,P.D. and Pavletich,N.P. (1994) Crystal structure of a p53 tumor suppressor–DNA complex: understanding tumorigenic mutations. *Science*, **265**, 346–355.
41. Iakoucheva,L.M., Brown,C.J., Lawson,J.D., Obradovic,Z. and Dunker,A.K. (2002) Intrinsic disorder in cell-signaling and cancer-associated proteins. *J. Mol. Biol.*, **323**, 573–584.
42. Bell,S., Klein,C., Muller,L., Hansen,S. and Buchner,J. (2002) p53 contains large unstructured regions in its native state. *J. Mol. Biol.*, **322**, 917–927.
43. Lee,H., Mok,K.H., Muhandiram,R., Park,K.H., Suk,J.E., Kim,D.H., Chang,J., Sung,Y.C., Choi,K.Y. and Han,K.H. (2000) Local structural elements in the mostly unstructured transcriptional activation domain of human p53. *J. Biol. Chem.*, **275**, 29426–29432.
44. Dawson,R., Muller,L., Dehner,A., Klein,C., Kessler,H. and Buchner,J. (2003) The N-terminal domain of p53 is natively unfolded. *J. Mol. Biol.*, **332**, 1131–1141.
45. Uversky,V.N. (2002) What does it mean to be natively unfolded? *Eur. J. Biochem.*, **269**, 2–12.
46. Uversky,V.N. (2002) Natively unfolded proteins: a point where biology waits for physics. *Protein Sci.*, **11**, 739–756.
47. Leiter,L.M., Chen,J., Marathe,T., Tanaka,M. and Dutta,A. (1996) Loss of transactivation and transrepression function and not RPA binding, alters growth suppression by p53. *Oncogene*, **12**, 2661–2668.
48. Henricksen,L.A., Umbricht,C.B. and Wold,M.S. (1994) Recombinant replication protein A: expression, complex formation and functional characterization. *J. Biol. Chem.*, **269**, 11121–11132.
49. Kay,L.E., Keifer,P. and Saarinen,T. (1992) Pure absorption gradient enhanced heteronuclear single quantum correlation spectroscopy with improved sensitivity. *J. Am. Chem. Soc.*, **114**, 10663.
50. Muhandiram,D.R. and Kay,L.E. (1994) Gradient-enhanced triple-resonance three-dimensional NMR experiments with improved sensitivity. *J. Magn. Reson. Ser. B*, **103**, 203–216.
51. Wittekind,M. and Mueller,L. (1993) HNCACB, a high-sensitivity 3D NMR experiment to correlate amide-proton and nitrogen resonances with the alpha- and beta-carbon resonances in proteins. *J. Magn. Reson. Ser. B*, **101**, 201–205.
52. Zhang,O., Kay,L.E., Olivier,J.P. and Forman-Kay,J.D. (1994) Backbone ^{1}H and ^{15}N resonance assignments of the N-terminal SH3 domain of drk in folded and unfolded states using enhanced-sensitivity pulsed field gradient NMR techniques. *J. Biomol. NMR*, **4**, 845–858.
53. Zhang,O., Kay,L.E., Olivier,J.P. and Forman-Kay,J.D. (1994) Backbone ^{1}H and ^{15}N resonance assignments of the N-terminal SH3 domain of drk in folded and unfolded states using enhanced-sensitivity pulsed field gradient NMR techniques. *J. Biomol. NMR*, **4**, 845.
54. Harris,R.B., Becker,E.D., Cabral De Menezes,S.M., Goodfellow,R. and Granger,P. (2001) NMR nomenclature. Nuclear spin properties and conventions for chemical shifts. *Pure Appl. Chem.*, **73**, 1795–1818.
55. Wishart,D.S., Bigam,C.G., Yao,J., Abildgaard,F., Dyson,H.J., Oldfield,E., Markley,J.L. and Sykes,B.D. (1995) ^{1}H, ^{13}C and ^{15}N chemical shift referencing in biomolecular NMR. *J. Biomol. NMR*, **6**, 135–140.
56. Kay,L.E., Torchia,D.A. and Bax,A. (1989) Backbone dynamics of proteins as studied by ^{15}N inverse detected heteronuclear NMR spectroscopy: application to staphylococcal nuclease. *Biochemistry*, **28**, 8972–8979.
57. Farrow,N.A., Zhang,O.W., Szabo,A., Torchia,D.A. and Kay,L.E. (1995) Spectral density-function mapping using N-15 relaxation data exclusively. *J. Biomol. NMR*, **6**, 153–162.
58. Lefevre,J.F., Dayie,K.T., Peng,J.W. and Wagner,G. (1996) Internal mobility in the partially folded DNA binding and dimerization domains of GAL4: NMR analysis of the N-H spectral density functions. *Biochemistry*, **35**, 2674–2686.
59. Peng,J.W. and Wagner,G. (1992) Mapping of the spectral densities of N-H bond motions in eglin c using heteronuclear relaxation experiments. *Biochemistry*, **31**, 8571–8586.
60. Peng,J.W. and Wagner,G. (1995) Frequency spectrum of NH bonds in eglin c from spectral density mapping at multiple fields. *Biochemistry*, **34**, 16733–16752.
61. Abragam,A. (1961) *The Principles of Nuclear Magnetism.* Clarendon Press, Oxford, pp. 315–316, 506–510.
62. Zuiderweg,E.R. (2002) Mapping protein-protein interactions in solution by NMR spectroscopy. *Biochemistry*, **41**, 1–7.
63. Wishart,D.S. and Case,D.A. (2001) Use of chemical shifts in macromolecular structure determination. *Methods Enzymol.*, **338**, 3–34.
64. Wishart,D.S. and Nip,A.M. (1998) Protein chemical shift analysis: a practical guide. *Biochem. Cell Biol.*, **76**, 153–163.
65. Wishart,D.S. and Sykes,B.D. (1994) Chemical shifts as a tool for structure determination. *Methods Enzymol.*, **239**, 363–392.

66. Wishart,D.S. and Sykes,B.D. (1994) The ^{13}C chemical-shift index: a simple method for the identification of protein secondary structure using ^{13}C chemical-shift data. *J. Biomol. NMR*, **4**, 171–180.
67. Dyson,H.J. and Wright,P.E. (2002) Insights into the structure and dynamics of unfolded proteins from nuclear magnetic resonance. *Adv. Protein Chem.*, **62**, 311–340.
68. Wright,P.E. and Dyson,H.J. (1999) Intrinsically unstructured proteins: re-assessing the protein structure–function paradigm. *J. Mol. Biol.*, **293**, 321–331.
69. Cavanagh,J., Faribrother,W.J., Palmer,A.G.,III and Skelton,N.J. (1996) *Protein NMR Spectroscopy: Principles and Practice*. Academic Press, San Diego, CA, pp. 291–299.
70. Bai,Y., Chung,J., Dyson,H.J. and Wright,P.E. (2001) Structural and dynamic characterization of an unfolded state of poplar apo-plastocyanin formed under nondenaturing conditions. *Protein Sci.*, **10**, 1056–1066.
71. Donne,D.G., Viles,J.H., Groth,D., Mehlhorn,I., James,T.L., Cohen,F.E., Prusiner,S.B., Wright,P.E. and Dyson,H.J. (1997) Structure of the recombinant full-length hamster prion protein PrP(29–231): the N terminus is highly flexible. *Proc. Natl Acad. Sci. USA*, **94**, 13452–13457.
72. Daughdrill,G.W., Hanely,L.J. and Dahlquist,F.W. (1998) The C-terminal half of the anti-sigma factor FlgM contains a dynamic equilibrium solution structure favoring helical conformations. *Biochemistry*, **37**, 1076–1082.
73. Yao,J., Chung,J., Eliezer,D., Wright,P.E. and Dyson,H.J. (2001) NMR structural and dynamic characterization of the acid-unfolded state of apomyoglobin provides insights into the early events in protein folding. *Biochemistry*, **40**, 3561–3571.
74. Wishart,D.S., Bigam,C.G., Holm,A., Hodges,R.S. and Sykes,B.D. (1995) ^{1}H, ^{13}C and ^{15}N random coil NMR chemical shifts of the common amino acids. I. Investigations of nearest-neighbor effects. *J. Biomol. NMR*, **5**, 67–81.
75. Kussie,P.H., Gorina,S., Marechal,V., Elenbaas,B., Moreau,J., Levine,A.J. and Pavletich,N.P. (1996) Structure of the MDM2 oncoprotein bound to the p53 tumor suppressor transactivation domain. *Science*, **274**, 948–953.
76. Dyson,H.J. and Wright,P.E. (2002) Coupling of folding and binding for unstructured proteins. *Curr. Opin. Struct. Biol.*, **12**, 54–60.
77. Lane,A.N. and Lefevre,J.F. (1994) Nuclear magnetic resonance measurements of slow conformational dynamics in macromolecules. *Methods Enzymol.*, **239**, 596–619.
78. Farrow,N.A., Zhang,O., Szabo,A., Torchia,D.A. and Kay,L.E. (1995) Spectral density function mapping using ^{15}N relaxation data exclusively. *J. Biomol. NMR*, **6**, 153–162.
79. Bentrop,D., Bertini,I., Iacoviello,R., Luchinat,C., Niikura,Y., Piccioli,M., Presenti,C. and Rosato,A. (1999) Structural and dynamical properties of a partially unfolded Fe4S4 protein: role of the cofactor in protein folding. *Biochemistry*, **38**, 4669–4680.
80. Mulder,F.A., Hon,B., Muhandiram,D.R., Dahlquist,F.W. and Kay,L.E. (2000) Flexibility and ligand exchange in a buried cavity mutant of T4 lysozyme studied by multinuclear NMR. *Biochemistry*, **39**, 12614–12622.
81. Nesmelova,I., Krushelnitsky,A., Idiyatullin,D., Blanco,F., Ramirez-Alvarado,M., Daragan,V.A., Serrano,L. and Mayo,K.H. (2001) Conformational exchange on the microsecond time scale in alpha-helix and beta-hairpin peptides measured by ^{13}C NMR transverse relaxation. *Biochemistry*, **40**, 2844–2853.
82. Kuhn,C., Muller,F., Melle,C., Nasheuer,H.P., Janus,F., Deppert,W. and Grosse,F. (1999) Surface plasmon resonance measurements reveal stable complex formation between p53 and DNA polymerase alpha. *Oncogene*, **18**, 769–774.
83. Binz,S.K., Sheehan,A.M. and Wold,M.S. (2004) Replication Protein A phosphorylation and the cellular response to DNA damage. *DNA Repair (Amst.)*, **3**, 1015–1024.
84. Binz,S.K., Lao,Y., Lowry,D.F. and Wold,M.S. (2003) The phosphorylation domain of the 32-kDa subunit of replication protein A (RPA) modulates RPA–DNA interactions. Evidence for an intersubunit interaction. *J. Biol. Chem.*, **278**, 35584–35591.
85. Wakasugi,M. and Sancar,A. (1999) Order of assembly of human DNA repair excision nuclease. *J. Biol. Chem.*, **274**, 18759–18768.